View metadata, citation and similar papers at core.ac.uk

brought to you by CORE

provided by University of Queensland eSpace

MOLECULAR AND CELLULAR BIOLOGY, July 2008, p. 4377–4385 Vol. 28, No. 13
0270-7306/08/$08.00+0 doi:10.1128/MCB.00050-08
Copyright © 2008, American Society for Microbiology. All Rights Reserved.

Electrostatic Interactions Positively Regulate K-Ras Nanocluster Formation and Function▽

Sarah J. Plowman,[1] Nicholas Ariotti,[1] Andrew Goodall,[1] Robert G. Parton,[1,2] and John F. Hancock[1]*

Institute for Molecular Bioscience, University of Queensland, St. Lucia, Brisbane 4072, Australia,[1] and Centre for Microscopy and Microanalysis, University of Queensland, St. Lucia, Brisbane 4072, Australia[2]

Received 10 January 2008/Returned for modification 18 February 2008/Accepted 18 April 2008

The organization of Ras proteins into plasma membrane nanoclusters is essential for high-fidelity signal transmission, but whether the nanoscale enviroments of different Ras nanoclusters regulate effector interactions is unknown. We show using high-resolution spatial mapping that Raf-1 is recruited to and retained in K-Ras–GTP nanoclusters. In contrast, Raf-1 recruited to the plasma membrane by H-Ras is not retained in H-Ras–GTP nanoclusters. Similarly, upon epidermal growth factor receptor activation, Raf-1 is preferentially recruited to K-Ras–GTP and not H-Ras–GTP nanoclusters. The formation of K-Ras–GTP nanoclusters is inhibited by phosphorylation of S181 in the C-terminal polybasic domain or enhanced by blocking S181 phosphorylation, with a concomitant reduction or increase in Raf-1 plasma membrane recruitment, respectively. Phosphorylation of S181 does not, however, regulate in vivo interactions with the nanocluster scaffold galectin-3 (Gal3), indicating separate roles for the polybasic domain and Gal3 in driving K-Ras nanocluster formation. Together, these data illustrate that Ras nanocluster composition regulates effector recruitment and highlight the importance of lipid/protein nanoscale environments to the activation of signaling cascades.

Ras proteins are involved in information transfer from cell surface receptors to intracellular signaling cascades. A critical feature of this process requires the nonrandom organization of Ras-GTP proteins on the inner leaflet of the plasma membrane (18, 19). Approximately 40% of Ras-GTP proteins are organized into nanoclusters comprising ~7 proteins; the remaining 60% of Ras-GTP proteins are randomly arrayed as monomers. This spatial distribution is essential for high-fidelity signal transmission from activated epidermal growth factor (EGF) receptor to the Raf/MEK/extracellular signal-regulated kinase (ERK) pathway (25).

The formation of nanoclusters involves a complex interplay between Ras membrane targeting motifs encoded by the C-terminal hypervariable region, the G domain, and cellular components such as plasma membrane lipid composition and the actin cytoskeleton (18–20, 22). For example, H-Ras, which is anchored by two palmitates and a farnesyl group, undergoes GTP-dependent lateral segregation between spatially distinct nanoclusters (18, 19). H-Ras–GDP forms cholesterol-dependent nanoclusters with radii of ~12 nm, while H-Ras–GTP forms cholesterol-independent nanoclusters with radii of 6 to 8 nm (18, 19). In contrast, K-Ras anchored by a farnesyl group and a polybasic domain forms actin-dependent, cholesterol-independent nanoclusters with radii of 6 to 8 nm (18, 19). Interaction of the K-Ras polybasic domain with the plasma membrane is likely to sequester acidic phospholipids in a manner analogous to the myristoylated alanine-rich C kinase substrate (MARCKS) protein (27). Therefore, the clustering of seven K-Ras proteins will result in a nanocluster environment highly enriched in acidic phospholipids. Consistent with this model, K-Ras membrane affinity can be modulated by changes to the overall charge of the polybasic domain via protein kinase C (PKC)-mediated phosphorylation of Ser181 (1).

The formation of Ras nanoclusters is essential for mitogen-activated protein kinase (MAPK) activation, in part because Raf-1 is recruited directly to K-Ras–GTP nanoclusters (25). Failure to form K-Ras–GTP nanoclusters therefore prevents signal transmission. Intriguingly, although the Ras binding domain (RBD) of Raf-1 binds with equivalent affinity to different Ras isoforms in vitro (12), there is a marked difference in the ability of Ras isoforms to activate Raf-1 in vivo (29). Specifically, K-Ras–GTP is a more potent activator of Raf-1 than H-Ras–GTP. Activation of the serine/threonine kinase Raf-1 is a complex process. The initial step requires recruitment of Raf-1 from the cytosol to the plasma membrane by Ras-GTP (14, 24), although the interaction of Raf-1 with acidic phospholipids, including phosphatidic acid and phosphatidylserine, appears important for more stable membrane interaction and activation (6, 7, 11, 16). Once localized to the plasma membrane, Raf-1 undergoes a series of phosphorylation and dephosphorylation events that activate the catalytic domain (reviewed in reference 28). Therefore, a number of functional elements are required within a Ras nanocluster to facilitate Raf-1 recruitment and activation.

Here we use immunoelectron microscopy (immuno-EM) and fluorescence lifetime imaging-fluorescent resonance energy transfer (FLIM-FRET) microscopy to explore the interaction of Raf-1 with different types of Ras nanocluster. Our findings demonstrate that the nanocluster environment is a critical regulator of Ras-effector interactions and illustrate the importance of understanding the lipid/protein nanoscale environment in which signaling cascades are assembled and activated.

* Corresponding author. Mailing address: Institute for Molecular Bioscience, University of Queensland, St. Lucia, Brisbane 4072, Australia. Phone: 61 7 3346 2033. Fax: 61 7 3346 2339. E-mail: j.hancock@imb.uq.edu.au.

▽ Published ahead of print on 5 May 2008.

Downloaded from http://mcb.asm.org/ on October 26, 2015 by University of Queensland Library

MATERIALS AND METHODS

Plasmids. Vectors expressing green fluorescent protein (GFP)–K-Ras, K-RasG12V, H-Ras, H-RasG12V, and monomeric red fluorescent protein (mRFP)–Raf-1 have been described previously (22, 25). GFP–K-RasG12V S181A and GFP–K-RasG12V S181D were generated by site-directed mutagenesis of GFP–K-RasG12V.

Antibodies and reagents. Reagents were purchased from the following suppliers: pan-Ras and Raf-1 antibodies from BD Transduction Labs; pMEK, pERK, and pSAPK from Cell Signaling Technologies; α-actin from Chemicon, Millipore; MitoTracker red CMXRos from Molecular Probes, Invitrogen; and EGF from Sigma-Aldridge.

Cell culture. BHK cells were maintained in HEPES-buffered Dulbecco's modified Eagle's medium containing 10% heat-inactivated serum supreme. BHK cells were seeded onto either glass-bottomed microwell dishes (MatTek Corporation) for microscopic analysis or 10-cm dishes for biochemical assays and transfected using Lipofectamine reagent (Invitrogen) according to the manufacturer's instructions as previously described (21). Where indicated, cells were serum starved for approximately 6 h and then stimulated for 30 s with the indicated concentration of EGF. Cells were incubated with MitoTracker red CMXRos for 30 min prior to imaging by confocal microscopy.

PC12 cells were cultured in Dulbecco's modified Eagle's medium supplemented with 5% horse serum, 10% fetal calf serum, and 2 mM L-glutamine. PC12 cells were seeded onto coverslips and following transfection were cultured in normal media for 3 days. Cells were fixed using 4% paraformaldehyde, and differentiation was determined microscopically. A minimum of 100 cells was counted for each condition.

EM and spatial mapping. Apical plasma membrane sheets were prepared, fixed with 4% paraformaldehyde–0.1% glutaraldehyde, and labeled with affinity-purified anti-GFP or anti-mRFP antiserum coupled directly to 5-nm gold particles as described previously (18, 19). For bivariate analysis, plasma membrane sheets were labeled sequentially with anti-mRFP antibody conjugated to 2-nm gold particles and anti-GFP antibody conjugated to 6-nm gold particles. Digital images of the immunogold-labeled plasma membrane sheets were taken at ×100,000 magnification in an electron microscope (Jeol 1011). Intact 1-μm^2 areas of the plasma membrane sheet were identified using Image J and the x and y coordinates of the gold particles were determined as described previously (18, 19). Bootstrap tests to examine differences between replicated point patterns were constructed exactly as described previously (4), and statistical significance was evaluated against 1,000 bootstrap samples.

FLIM-FRET microscopy. FLIM experiments were carried out using a lifetime fluorescence imaging attachment (Lambert Instruments, Leutingewolde, The Netherlands) on an inverted microscope (Olympus IX71). BHK cells transiently expressing either mGFP–H-RasG12V or mGFP–K-RasG12V (donor), alone or with mRFP–Raf-1 (acceptor) (using a 1:3 ratio of plasmid DNA), were excited using a sinusoidally modulated 3-W 470-nm light-emitting diode at 80 MHz under epi-illumination. Fluorescein was used as a lifetime reference standard. Cells were imaged with a ×60 1.45-numerical-aperture oil objective using an appropriate GFP filter set. The phase and modulation were determined from a set of 12 phase settings using the manufacturer's software. Resolution of two lifetimes in the frequency domain was performed using a graphical method (3) mathematically identical to global analysis algorithms (5, 26). The analysis yields the mGFP lifetime of free mGFP donor (τ_1) and the mGFP lifetime in donor acceptor complexes (τ_2) and estimates the fraction of mGFP in donor-acceptor complexes (α). Analysis was performed on a cell-by-cell basis. Average FRET efficiency ($= 1 - \tau_2/\tau_1$) was 53.4% ± 1.35% (mean ± standard error of the mean [SEM]). To quantify the fraction of mRFP without a functional chromophore, we performed FLIM measurements on BHK cells expressing an mGFP-mRFP fusion protein and obtained a value of $\alpha = 0.55 \pm 0.05$ (mean ± SEM). Our estimates of FRET fraction take this into account.

Confocal microscopy. BHK cells grown in 35-mm glass-bottomed microwell dishes were imaged live using a Zeiss LSM 510 confocal microscope with a heated stage attachment, using the appropriate GFP and Mitotracker red CMXRos filter sets.

Western blotting. Cells were washed and subjected to hypotonic lysis, and P100 and S100 fractions were prepared from postnuclear supernatant as described previously (2). To measure the relative abundance of Ras and Raf-1 in cellular equivalents of the P100 fraction and the S100 fraction, a total of 20 μg of each P100 fraction and an equal proportion of the S100 fraction were immunoblotted. For analysis of signal transduction, whole-cell lysates were produced (50 mM Tris [pH 7.5], 75 mM NaCl, 25 mM NaF, 5 mM $MgCl_2$, 5 mM EGTA, 1 mM dithiothreitol, 100 μM $NaVO_4$, 1% Nonidet P-40 plus protease inhibitors) and a total of 20 μg of each was immunoblotted with pan-Ras, pMEK, pERK, and pSAPK antibodies. The α-actin antibody labeling was used as a loading control. Signal was detected by enhanced chemiluminescence (Pierce) and imaged by Lumi-Imager (Roche). Quantification of intensities was performed using Image J.

RESULTS

Constitutively active Ras isoforms differentially regulate Raf-1 plasma membrane recruitment. To address the role of different Ras nanocluster environments in regulating effector recruitment, we first investigated the distribution of GFP–Raf-1 by EM spatial mapping. Intact sheets of apical plasma membrane were generated and immunogold labeled using anti-GFP antibodies conjugated directly to 5-nm gold particles to detect GFP–Raf-1. In serum-starved cells, in the absence of constitutively active Ras, only a low basal level of immunogold labeling was detected (Fig. 1A). However, expression of either mRFP–H-RasG12V or mRFP–K-RasG12V resulted in a substantial increase in Raf-1 membrane recruitment (Fig. 1A). By measuring the level of immunogold labeling, we determined that mRFP–K-RasG12V recruited significantly more ($P = 0.02$) GFP–Raf-1 to the plasma membrane than mRFP–H-RasG12V despite both isoforms being GTP loaded (Fig. 1A). Plasma membrane sheets were labeled with anti-mRFP 5-nm gold particles to detect the relative expression of mRFP–K-RasG12V and mRFP–H-RasG12V in these experiments (data not shown). After correction for the difference in K-RasG12V and H-RasG12V expression levels, we calculate that K-RasG12V recruits fivefold more Raf-1 than does an equivalent level of H-RasG12V. Spatial point pattern analysis of the immunogold patterns revealed that GFP–Raf-1 was organized into nanoclusters with radii of 24 to 26 nm. The spatial distributions of these Raf-1 nanoclusters were not significantly different ($P = 0.783$) (Fig. 1B). In previous work, we calibrated the radius (r) of the maximum value of $L(r) - r$ against model in vitro domains (18). Applying the same calibration here, we estimate the lower bound for the radius of the Raf-1 nanocluster to be in the range of ~14 to 16 nm. Thus, the expression of either H-RasG12V or K-RasG12V is sufficient to drive Raf-1 membrane recruitment and nanoclustering, albeit to different extents.

The K-Ras–GTP nanocluster is one site of Raf-1 recruitment (25). The data in Fig. 1A to C suggest that Raf-1 may also be recruited to H-Ras–GTP nanoclusters. To validate this interpretation, plasma membrane sheets derived from cells expressing mRFP–H-RasG12V and GFP–Raf-1 or mRFP–K-RasG12V and GFP–Raf-1 were labeled with different sizes of gold particles (2 or 6 nm) and the immunogold point patterns were quantified by a bivariate analysis. The results confirmed that mRFP–K-RasG12V and GFP–Raf-1 colocalize in the mRFP–K-RasG12V nanocluster (Fig. 1C). Based on the level of immunogold labeling, the known antibody capture ratio, and the number of Ras proteins per cluster (18), we estimate, by fitting a Poisson distribution, that ~66% of K-RasG12V nanoclusters recruit three to six Raf-1 proteins, with a mean of 3.5 per nanocluster. In contrast, however, the equivalent bivariate analysis showed no significant colocalization between mRFP–H-RasG12V and GFP–Raf-1 on the plasma membrane. Taken together, these data suggest that H-RasG12V recruits Raf-1 to

Downloaded from http://mcb.asm.org/ on October 26, 2015 by University of Queensland Library

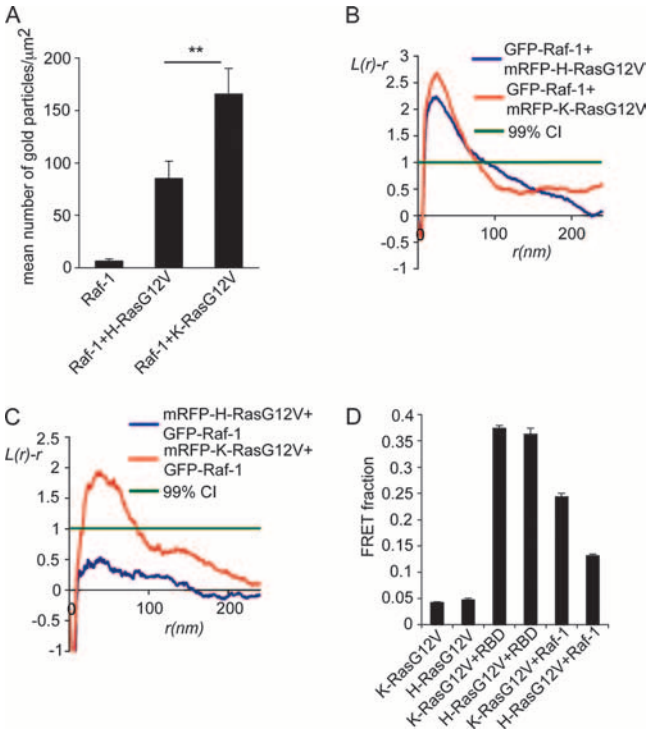

FIG. 1. Raf-1 is recruited to K-Ras–GTP nanoclusters but not H-Ras–GTP nanoclusters. (A) Plasma membrane sheets generated from BHK cells expressing GFP–Raf-1 alone or in the presence of mRFP–H-RasG12V or mRFP–K-RasG12V were labeled with anti-GFP antibodies conjugated to 5-nm gold particles. The graph shows the mean number of gold particles/μm^2 ($\pm$SEM; $n = 6$, 17, and 14, respectively). Significant differences were assessed using t tests (**, $P < 0.02$). (B) The spatial distribution of the gold labeling generated in panel A was analyzed. Maximum $L(r) - r$ values above the 99% confidence interval (CI) for complete spatial randomness indicate clustering at the value of r. Univariate K-functions are weighted means ($n \geq 9$) standardized on the 99% CI. Significant differences were assessed using bootstrap tests. The formation of Raf-1 nanoclusters following recruitment by either H-RasG12V or K-RasG12V is not significantly different ($P = 0.783$). (C) Plasma membrane sheets generated from BHK cells expressing GFP–Raf-1 in the presence or absence of mRFP–H-RasG12V or mRFP–K-RasG12V were colabeled with anti-mRFP and anti-GFP antibodies conjugated to 2-nm and 6-nm gold particles, respectively. Bivariate analyses were performed to determine if the two gold populations colocalized. $L(r) - r$ curves above the 99% CI showed significant colocalization. The K-functions are means ($n = 8$) standardized on the 99% CI. (D) FLIM-FRET detects protein-protein interactions through measurement of changes in the fluorescence lifetime of the donor fluorophore (mGFP) in the presence of the acceptor fluorophore (mRFP). BHK cells coexpressing (i) mGFP–H-RasG12V in the presence or absence of mRFP-RBD or mRFP–Raf-1 and (ii) mGFP–K-RasG12V in the presence or absence of mRFP-RBD or mRFP–Raf-1 were imaged in the frequency domain in a wide-field FLIM microscope. Global analysis and calibration with an mGFP-mRFP fusion protein were used to calculate the fraction of mGFP–K-RasG12V and mGFP–H-RasG12V molecules undergoing FRET. Error bars show the SEM ($n = 26$ to 106).

the plasma membrane but that Raf-1 is not efficiently retained in H-RasG12V nanoclusters.

To determine whether the effector binding domains of H-RasG12V and K-RasG12V are equally accessible to recruit cytosolic Raf-1, we used FLIM-FRET microscopy to analyze the interaction of mRFP-RBD with mGFP–H-RasG12V and mGFP–K-RasG12V. FLIM-FRET quantifies the proximity of two proteins through the measurement of changes in the fluorescence lifetime of the donor fluorophore (mGFP), when it interacts with the acceptor fluorophore mRFP. Figure 1D shows a similar FRET fraction of ~40% for both mGFP–K-RasG12V and mGFP–H-RasG12V when coexpressed with an excess of mRFP-RBD. This result indicates that the extent of the interaction between the RBD and K-RasG12V is equivalent to that of H-RasG12V. The FRET fraction of 40% also correlates with the fraction of Ras-GTP molecules that are in nanoclusters (18). In contrast, when we examined the interaction between full-length mRFP–Raf-1 and either mGFP–H-RasG12V or mGFP–K-RasG12V we detected a significant difference between the mGFP FRET fractions. A larger fraction of mGFP–K-RasG12V (24.4% $\pm$ 0.7%) than of H-RasG12V (13.1% $\pm$ 0.3%) interacted with full-length mRFP–Raf-1 (Fig. 1D). These data correlate closely with the immuno-EM data and suggest that domains within Raf-1 that are absent from the minimal RBD may regulate the differential interaction with different Ras nanoclusters.

K-Ras but not H-Ras recruits Raf-1 to plasma membrane nanoclusters in response to EGF stimulation. Taken together, the data in Fig. 1 demonstrate that Raf-1 is efficiently recruited to and retained in K-RasG12V but not H-RasG12V nanoclusters. However, these experiments were all carried out with K-Ras and H-Ras proteins that are constitutively GTP loaded by virtue of an oncogenic G12V mutation. We therefore used EM spatial mapping to quantify the de novo recruitment of Raf-1 to Ras-GTP nanoclusters generated in response to EGF stimulation. In serum-starved cells, in the absence of EGF, only a very low level of Raf-1 was present on the plasma membrane (Fig. 2A) and this was not altered by exogenous expression of K-Ras (Fig. 2B). EGF stimulation of cells expressing mRFP–K-Ras and GFP–Raf-1, or mRFP–H-Ras and GFP–Raf-1, stimulated Raf-1 membrane recruitment that was readily detected by immunogold labeling. EGF-stimulated cells expressing K-Ras recruited significantly more Raf-1 to the plasma membrane than did cells expressing an equivalent level of H-Ras ($P < 0.001$) (Fig. 2A). Spatial analysis of the immunogold pattern revealed that following recruitment by K-Ras–GTP, Raf-1 was organized into nanoclusters with an observed radius of 25 nm (Fig. 2C), corresponding to an estimated lower bound of ~15 nm. Due to the low level of Raf-1 recruited in H-Ras-expressing cells, we were unable analyze its spatial distribution. Taken together, these data and those in Fig. 1 show that EGF specifically stimulates the recruitment of Raf-1 to K-Ras–GTP nanoclusters in BHK cells.

We have shown that there is a linear relationship between EGF concentration and the number of K-Ras–GTP nanoclusters formed (25). We show here that Raf-1 is primarily recruited to K-Ras nanoclusters in response to EGF stimulation: taken together, these results predict that Raf-1 recruitment to K-Ras nanoclusters should also be directly proportional to the level of EGF stimulation. To formally test this hypothesis, we used EM spatial mapping to analyze Raf-1 recruitment to K-Ras nanoclusters in response to different concentrations of EGF. Figure 2D confirms a linear relationship between the amount of Raf-1 recruited to K-Ras nanoclusters and EGF concentration ($R^2 = 0.9998$).

Downloaded from http://mcb.asm.org/ on October 26, 2015 by University of Queensland Library

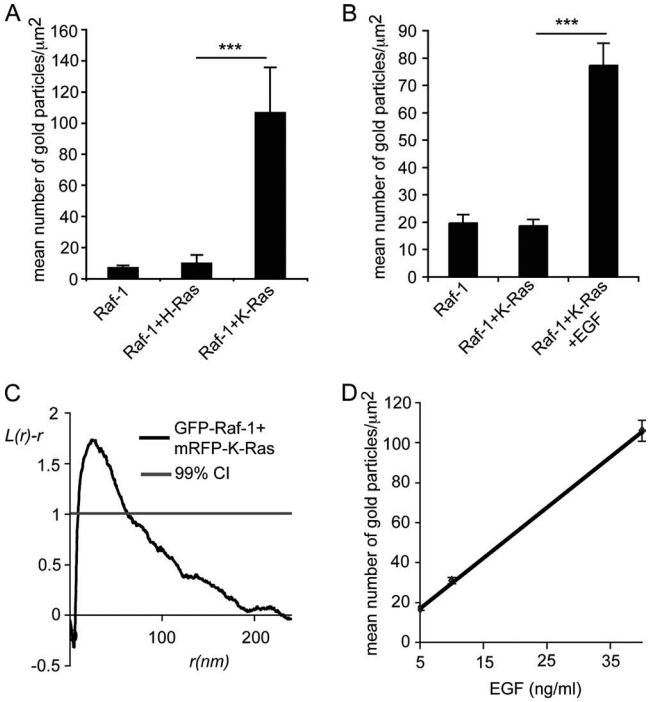

FIG. 2. Raf-1 is preferentially recruited to plasma membrane nanoclusters by K-Ras–GTP following EGF stimulation. (A) BHK cells expressing GFP–Raf-1, mRFP–H-Ras, and GFP–Raf-1 and mRFP–K-Ras and GFP–Raf-1 were serum starved for 6 h and then stimulated with 40 ng/ml EGF for 30 s. Plasma membrane sheets were generated and labeled with anti-GFP antibody conjugated to 5-nm gold particles. Error bars show the SEM ($n \geq 8$). Significant differences were assessed by t test (***, $P < 0.001$). (B) BHK cells expressing GFP–Raf-1 or mRFP–K-Ras and GFP–Raf-1 were serum starved for 6 h and then stimulated with 40 ng/ml EGF for 30 s. Plasma membrane sheets were generated and labeled with anti-GFP antibody conjugated to 5-nm gold particles. Error bars show the SEM ($n = 12$). Significant differences were assessed by t test (***, $P < 0.001$). (C) The spatial distribution of Raf-1 recruited by K-Ras following stimulation with 40 ng/ml EGF for 30 s in panel A was analyzed. K-functions are means ($n = 8$) standardized on the 99% confidence interval (CI). (D) Plasma membrane sheets were generated from BHK cells expressing mRFP–K-Ras and GFP–Raf-1 that had been stimulated with the indicated concentration of EGF for 30 s. The plasma membrane sheets were labeled with anti-GFP antibody conjugated to 5-nm gold particles. Error bars show the SEM. $R^2 = 0.9998$.

K-Ras–GTP nanocluster formation is highly sensitive to the net charge of the polybasic domain. The polybasic domain of K-Ras mediates membrane association via electrostatic interactions (10, 15) that can be disrupted by PKC-mediated phosphorylation of Ser181 (1). To explore the relationship between the net charge of the polybasic domain and K-Ras nanocluster formation, we generated a phosphomimetic mutant (S181D) and a control nonphosphorylated mutant (S181A) (1). Cellular fractionation experiments showed no significant differences in the extent of membrane (P100) binding of GFP–K-RasG12V and GFP–K-RasG12V S181A ($P = 0.35$), whereas a greater fraction of GFP–K-RasG12V S181D was cytosolic (S100) compared to GFP–K-RasG12V ($P = 0.016$) (Fig. 3A). These results are consistent with the introduction of a negative charge at Ser181 reducing the stability of K-RasG12V membrane binding. The GFP–K-RasG12V and GFP–K-RasG12V S181A constructs were localized predominantly to the plasma membrane when imaged live in BHK cells (Fig. 3B). Similarly, although a fraction of GFP–K-RasG12V S181D was associated with intracellular membranes, including mitochondria, as previously shown (1), the majority was associated with the plasma membrane. Thus, we were able to investigate whether a negative charge at Ser181 influenced nanocluster formation in BHK cells in addition to reducing K-Ras membrane affinity.

Immunogold labeling of plasma membrane sheets labeled with anti-GFP antibodies showed that the nanoclustering of GFP–K-RasG12V S181D was significantly reduced compared to that of K-RasG12V ($P = 0.042$) (Fig. 3C). The radius of the GFP–K-RasG12V S181D clusters was unchanged, but the peak value of the $L(r) - r$ function was decreased, indicative of a reduction in the clustered fraction. Conversely, an analysis of the immunogold point patterns of GFP–K-RasG12V S181A showed a significant increase in nanoclustering ($P = 0.001$) compared to GFP–K-RasG12V (Fig. 3C). In the same experiments, we also detected increased membrane association of GFP–K-RasG12V S181A compared to GFP–K-RasG12V and GFP–K-RasG12V S181D, as evidenced by significantly greater immunogold labeling. This result is consistent with the results of cell fractionation experiments and again indicates that GFP–K-RasG12V S181A is more stably associated with the plasma membrane than K-RasG12V S181D is.

We reasoned that the increased nanoclustering of K-RasG12V S181A compared to that of K-RasG12V may reflect endogenous PKC activity, resulting in a fraction of K-RasG12V being phosphorylated on Ser181. To explore this possibility more rigorously, we treated BHK cells expressing GFP–K-RasG12V with bryostatin at a concentration previously shown to induce PKC phosphorylation of K-Ras (1). EM spatial mapping showed a significant decrease in K-RasG12V nanocluster formation following bryostatin treatment that was also associated with decreased K-RasG12V membrane binding (Fig. 3D). These data suggest that PKC may act as a physiological regulator of K-Ras nanocluster formation as well as K-Ras membrane affinity.

Altered K-Ras nanocluster formation does not correlate with altered Gal3 function. The β-galactoside binding protein galectin-3 (Gal3) functions as a critical scaffold for the formation of K-Ras–GTP nanoclusters. Exogenous expression of Gal3 increases K-Ras–GTP nanocluster formation, while Gal3 knockdown abrogates K-Ras–GTP nanocluster formation (R. Shalom-Feuerstein, S. Plowman, B. Rotblat, N. Ariotti, T. Tian, J. Hancock, and Y. Kloog, unpublished data). We therefore examined whether the regulation of nanocluster formation by phosphorylation of S181 was effected through Gal3 interaction with K-Ras. Spatial analysis of plasma membrane sheets generated from cells expressing GFP–K-RasG12V, GFP–K-RasG12V S181A, and GFP–K-RasG12V S181D in the presence or absence of mRFP-Gal3 showed that coexpression of mRFP-Gal3 significantly increased K-RasG12V nanocluster formation, irrespective of the amino acid at position 181 (Fig. 4). We conclude from this result that phosphorylation of Ser181 does not regulate the scaffolding function of Gal3.

Modulation of the number of K-Ras–GTP nanoclusters directly alters the functional output. Next, we explored the relationship between K-Ras nanocluster formation and functional output. We initially analyzed Raf-1 recruitment from

Downloaded from http://mcb.asm.org/ on October 26, 2015 by University of Queensland Library

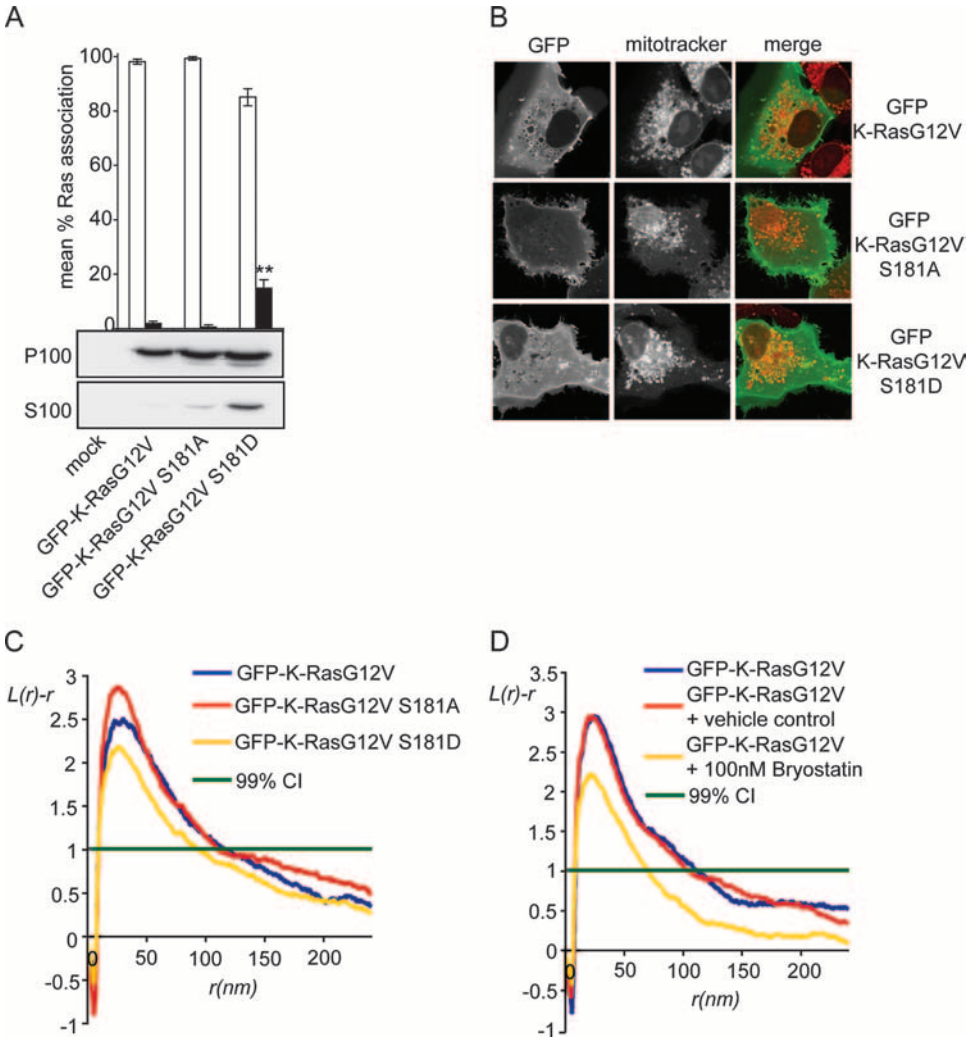

FIG. 3. K-Ras–GTP membrane affinity and nanocluster formation are directly modulated by the charge at position 181. (A) Membrane (P100) and soluble (S100) fractions were generated from BHK cells either mock transfected with empty vector or transfected with GFP–K-RasG12V, GFP–K-RasG12V S181A, and GFP–K-RasG12V S181D and probed with a pan-Ras antibody. To quantify the relative distributions of the K-Ras proteins, cellular equivalents of P100 and S100 fractions were analyzed. The graph shows the mean percentage of P100 and S100 Ras association (±SEM; $n = 3$). Significant differences from control GFP–K-RasG12V were assessed using t tests (**, $P < 0.02$). Bars: white, P100; black, S100. (B) Representative confocal images of BHK cells expressing GFP–K-RasG12V, GFP–K-RasG12V S181A, and GFP–K-RasG12V S181D. Cells were incubated with MitoTracker red CMXRos for 30 min prior to imaging. (C) Plasma membrane sheets generated from BHK cells expressing GFP–K-RasG12V, GFP–K-RasG12V S181A, and GFP–K-RasG12V S181D were labeled with anti-GFP antibodies conjugated to 5-nm gold particles. K-functions are weighted means ($n \geq 10$) standardized on the 99% confidence interval (CI). Significant differences from control K-RasG12V patterns were assessed using bootstrap tests. The mean numbers of gold particles/μm^2 were calculated for K-RasG12V, K-RasG12V S181A, and K-RasG12V S181D (151 ± 16, 251 ± 38, and 151 ± 16 gold particles/μm^2, respectively). Significant differences from control K-RasG12V levels were assessed by t test ($P = 0.024$ and 1, respectively). (D) BHK cells expressing GFP–K-RasG12V were either untreated, treated with vehicle alone, or treated with 100 nM bryostatin. Plasma membrane sheets were generated and labeled with anti-GFP antibodies conjugated to 5-nm gold particles. K-functions are weighted means ($n = 9$ to 12) standardized on the 99% CI. Significant differences from control K-RasG12V patterns were assessed using bootstrap tests ($P = 1$ and 0.001 for vehicle control and bryostatin treatment, respectively).

cytosol to membrane. Cell fractionation showed that the overall Raf-1 membrane (P100) recruitment was not significantly altered by mutation of Ser181 to either alanine or aspartic acid ($P = 0.98$ and 0.95, respectively) (Fig. 5A). We went on to precisely quantify the degree of interaction between mRFP–Raf-1 and the GFP–K-RasG12V proteins using FLIM-FRET microscopy. In line with the cellular fractionation experiments, the results showed that mRFP–Raf-1 interacted similarly with GFP–K-RasG12V, GFP–K-RasG12V S181A, and GFP–K-RasG12V S181D (Fig. 5B), although we observed a small but significantly enhanced interaction of mRFP–Raf-1 with K-RasG12V S181A compared to K-RasG12V S181D. Finally, we examined how Raf-1–K-RasG12V interactions were modulated at the level of the K-Ras–GTP nanocluster. EM spatial mapping of plasma membrane sheets labeled with anti-mRFP antibodies revealed more extensive nanoclustering of mRFP–Raf-1 following recruitment by GFP–K-RasG12V S181A than following recruitment by either GFP–K-RasG12V or GFP–K-RasG12V S181D (Fig. 5C).

Taken together, the results in Fig. 3 to 5 show that mutation

Downloaded from http://mcb.asm.org/ on October 26, 2015 by University of Queensland Library

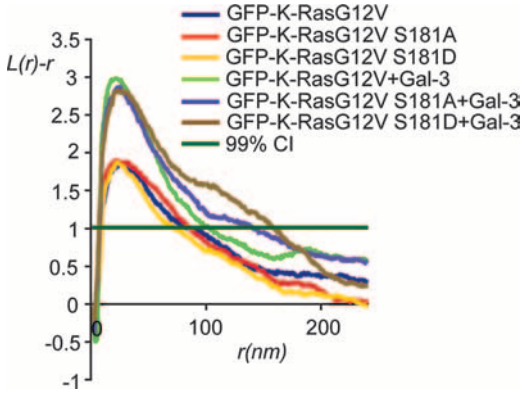

FIG. 4. Gal3 regulates K-Ras–GTP nanocluster formation. Plasma membrane sheets generated from cells expressing GFP–K-RasG12V, GFP–K-RasG12V S181A, and GFP–K-RasG12V S181D in the presence or absence of mRFP-Gal3 (1:3 ratio) were labeled with anti-GFP conjugated to 5-nm gold particles. K-functions are weighted means (n = 10 to 12) standardized on the 99% confidence interval (CI). Significant differences from control GFP–K-RasG12V patterns were assessed using bootstrap tests.

of Ser181 to alanine stabilizes the K-RasG12V signaling nanocluster, leading to a concomitant increase in Raf-1 nanoclustering. To address whether the observed changes in Raf-1 nanoclustering correlate with altered signal output, we analyzed the activation of components of the Raf/MEK/ERK pathway. Higher levels of ppMEK, ppERK, and ppSAPK were detected in cells expressing GFP–K-RasG12V S181A compared to those in cells expressing GFP–K-RasG12V (Fig. 6A). Interestingly, however, we detected similar increases of pMEK, pERK, and pSAPK in cells expressing GFP–K-RasG12V S181D. To determine whether the elevated activation of the Raf/MEK/ERK pathway translated into a measurable biological outcome, we utilized the PC12 differentiation assay. Expression of GFP–K-RasG12V S181D promoted PC12 differentiation to a greater extent than did expression of GFP–K-RasG12V ($P < 0.001$) (Fig. 6B), consistent with increased activation of the Raf/MEK/ERK pathway. Unexpectedly, the increased activation of ppMEK and ppERK induced by K-RasG12V S181A did not translate into increased PC12 cell differentiation.

DISCUSSION

Ras nanoclusters serve as platforms for the assembly of signaling complexes and play a critical role in generating high-fidelity signal transduction across the plasma membrane (25). Here we explored in detail the operation of Ras-GTP nanoclusters with respect to effector recruitment and observed striking differences between the interaction of Raf-1 with H-Ras–GTP and K-Ras–GTP nanoclusters. Consistent with in vitro biochemical studies (12), we find that the RBD interacts equivalently with H-Ras–GTP and K-Ras–GTP. Constitutively active RasG12V is >90% GTP loaded; however, in intact cells we observed a FRET fraction of only ~40% between the RBD and both H-RasG12V and K-RasG12V isoforms. Interestingly, this fraction is approximately equal to the fraction of Ras-GTP found in nanoclusters (18). Taken together with previous observations that Ras nanoclusters are the actual sites of effector recruitment (9, 13, 17, 25), we propose that the RBD may interact only with those Ras-GTP proteins that are resident in nanoclusters. A possible molecular basis for this interpretation flows from recent molecular dynamics simulations of H-Ras on a model lipid bilayer (8). This study showed two possible orientations of the G domain with respect to the plane of the membrane, resulting in differential display of the effector loop to the cytosol. We speculate therefore that the organization of Ras proteins into nanoclusters may facilitate effector recruitment by stabilizing a conformation of Ras-GTP in which the effector-binding domain is orientated toward the cytosol.

Despite the ability of H-Ras–GTP and K-Ras–GTP to interact equivalently with the RBD, K-Ras–GTP recruits fivefold more full-length Raf-1 than H-Ras–GTP does. Furthermore, EM and FLIM-FRET imaging show that full-length Raf-1 remains associated with K-Ras nanoclusters to a significantly greater extent than with H-Ras nanoclusters. One interpretation of these results is that the nanoscale protein/lipid environment of K-Ras nanoclusters provides a higher-affinity binding platform for full-length Raf than do H-Ras nanoclusters. Thus, although Raf-1 proteins are recruited equivalently to both types of Ras nanocluster, Raf-1 proteins are efficiently retained only in K-Ras nanoclusters. The basis of this high-affinity interaction may be the local remodeling of the lipid bilayer that results from the formation of a K-Ras nanocluster. Since K-Ras membrane association is mediated through the electrostatic interaction of the polybasic domain with the plasma membrane (23), binding of the K-Ras polybasic domain to the plasma membrane will sequester acidic phospholipids in a manner analogous to the MARCKS protein (27). This effect is amplified by the assembly of a K-Ras nanocluster composed of seven K-Ras proteins, leading to the formation of a local environment highly enriched in acidic phospholipids. Given that Raf-1 binds with high affinity to phosphatidylserine and phosphatidic acid (6, 7, 11, 16), such an acidic lipid environment would be expected to provide a localized high-affinity binding domain that is optimized for Raf-1 activation.

Our data suggest that H-Ras–GTP recruits Raf-1 to the plasma membrane but that Raf-1 is unable to engage in high-affinity interactions with the H-Ras–GTP nanocluster and, as such, Raf-1 recruitment is transient. Intriguingly, following release from the H-Ras–GTP nanocluster, Raf-1 maintains sufficient membrane affinity to enable nanocluster formation. How these H-Ras-independent Raf-1 nanoclusters are formed is currently unknown. It is conceivable that the high-affinity binding of Raf-1 to phosphatidylserine and phosphatidic acid (6, 7, 11, 16) is sufficient to allow transient nanoclustering to occur. However, further work is required to address the role of Raf-1 phospholipid binding in membrane recruitment and nanocluster formation.

In further support of a role for lipid remodeling in promoting high-affinity Raf-1 interaction with K-Ras nanoclusters, we show that the formation of K-Ras–GTP nanoclusters is sensitive to the net charge of the polybasic domain and specifically is inversely correlated with the presence of a negative charge on Ser181. Thus, the formation of K-Ras–GTP nanoclusters is inhibited either by mutation (S181D) or by PKC phosphorylation of Ser181. The introduction of a negative charge into the polybasic domain may perturb the recruitment of acidic phospholipids, reducing the stability of K-Ras membrane interac-

Downloaded from http://mcb.asm.org/ on October 26, 2015 by University of Queensland Library

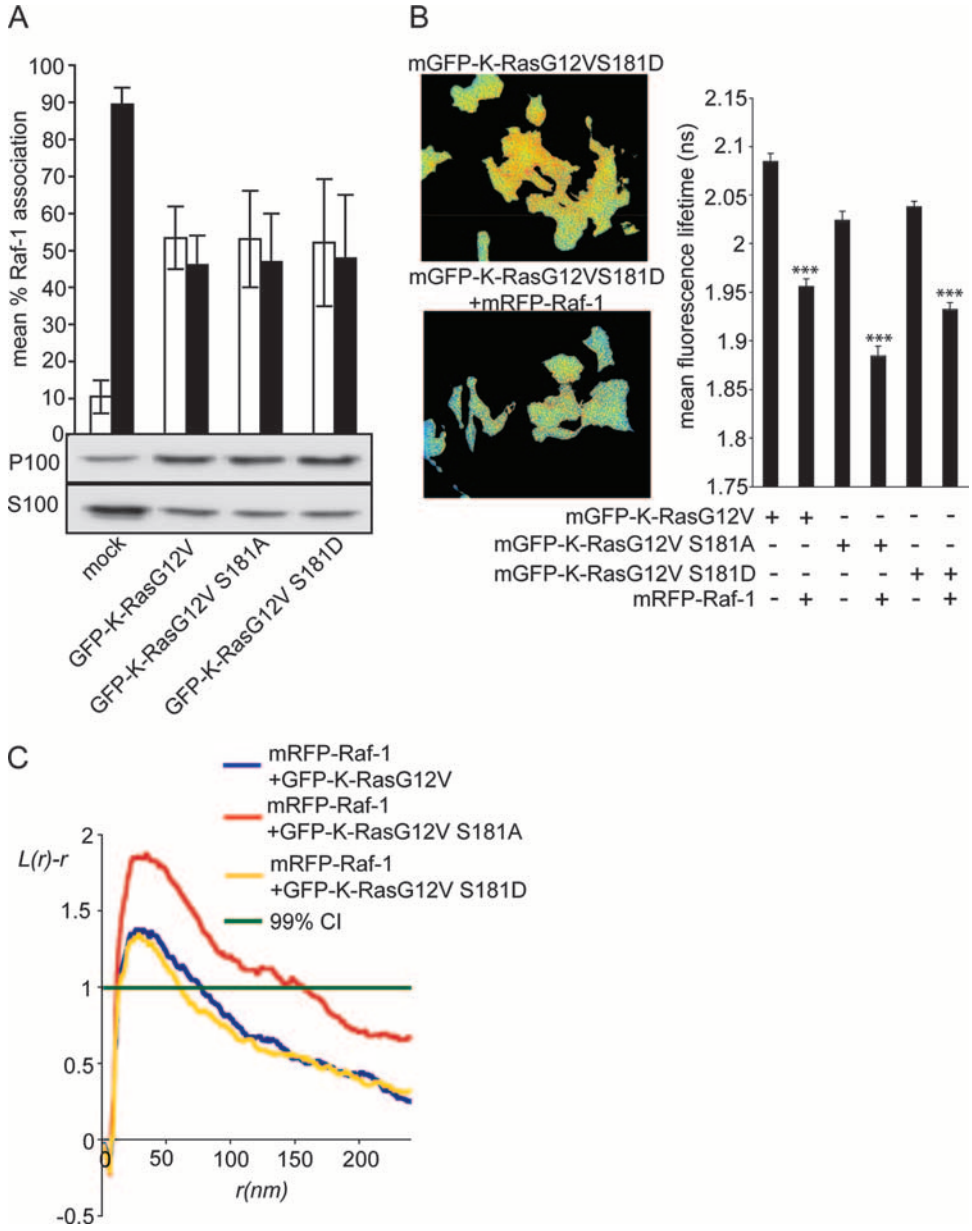

FIG. 5. Raf-1 recruitment is sensitive to changes in K-Ras–GTP nanocluster formation. (A) Membrane (P100) and soluble (S100) fractions were generated from BHK cells either mock transfected or expressing GFP–K-RasG12V, GFP–K-RasG12V S181A, and GFP–K-RasG12V S181D and blotted with an anti-Raf-1 antibody. To quantify the relative distribution of Raf-1, cellular equivalents of P100 and S100 fractions were analyzed. Bars represent the mean percentage of Raf-1 associated with the P100 and S100 fractions (±SEM; $n = 3$) with a representative blot. Bars: white, P100; black, S100. Significant differences from the control were assessed using a t test. (B) Raf-1 recruitment to K-Ras nanoclusters was assessed by FLIM-FRET microscopy. Representative images of the fluorescence lifetime of the donor fluorophore mGFP in the absence or presence of the acceptor fluorophore mRFP are shown. Bars represent the mean fluorescence lifetime of mGFP pooled from three independent experiments (±SEM; $n \geq 62$). Significant differences from control cells not expressing the acceptor fluorophore were assessed using t tests (***, $P < 0.001$). The differences observed in the mGFP fluorescence lifetimes in the absence of acceptor fluorophore may reflect changes in intracellular conditions such as pH induced by GFP–K-RasG12V S181A and GFP–K-RasG12V S181D compared to GFP–K-RasG12V. (C) Recruitment of Raf-1 to K-RasG12V nanoclusters was assessed by immuno-EM. Plasma membrane sheets generated from BHK cells expressing (i) GFP–K-RasG12V and mRFP–Raf-1, (ii) GFP–K-RasG12V S181A and mRFP-Raf-1, or (iii) GFP–K-RasG12V S181D and mRFP–Raf-1 were labeled with anti-mRFP antibodies conjugated to 5-nm gold particles. K-functions are weighted means ($n \geq 8$) standardized on the 99% confidence interval (CI). Significant differences from control K-RasG12V–Raf patterns were assessed using bootstrap tests.

tion and decreasing the probability of nanocluster formation. It is clear, however, that phosphorylation of the polybasic domain does not affect the nanocluster scaffold function of Gal3, since ectopic expression of Gal3 is equally potent at increasing nanocluster formation by K-RasG12V S181D and K-RasG12V S181A. Thus, the polybasic domain and bound Gal3 appear to operate as independent determinants for K-Ras–plasma membrane interactions. Interestingly, we observed a close correla-

Downloaded from http://mcb.asm.org/ on October 26, 2015 by University of Queensland Library

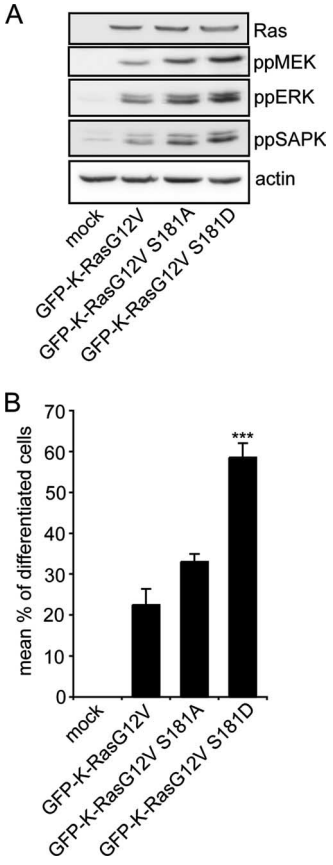

FIG. 6. Signal output from the MAPK pathways is modulated by K-Ras nanocluster formation. (A) Whole-cell lysates were generated from cells either mock transfected or expressing GFP–K-RasG12V, GFP–K-RasG12V S181A, and GFP–K-RasG12V S181D. Lysates were blotted for Ras, ppMEK, ppERK, and ppSAPK. Actin was used as a loading control. Representative blots are shown ($n = 3$). (B) PC12 cells either mock transfected with empty vector or transfected with GFP–K-RasG12V, GFP–K-RasG12V S181A, and GFP–K-RasG12V S181D were cultured for 3 days, and differentiation was scored. Error bars represent the SEM ($n = 3$). Significant differences from control K-RasG12V-transfected cells were assessed using t tests (***, $P < 0.001$).

tion between K-Ras membrane affinity and the formation of K-Ras nanoclusters. Thus, K-RasG12V S181D exhibited reduced membrane affinity and a lower clustered fraction than K-RasG12V S181A. We conclude that K-Ras proteins within nanoclusters have a higher affinity for the plasma membrane than monomeric randomly arrayed K-Ras proteins, perhaps reflecting the combined effect of Gal3 driving K-Ras into nanoclusters that then facilitate acidic phospholipid sequestration.

Regulation of K-Ras nanocluster formation by manipulation of the net polybasic domain charge has complex effects on signal output and biological function. Consistent with the role of the K-Ras–GTP nanocluster in generating high-fidelity signal transmission (25), the increased signal output from K-RasG12V S181A correlated closely with increased nanocluster formation and increased Raf-1 nanocluster recruitment. However, the increased signal output from K-RasG12V S181A is not translated into a significant increase in PC12 cell differentiation. These data suggest that K-RasG12V generates a level of signal output from plasma membrane nanoclusters that is above the threshold required to achieve maximal differentiation. Thus, the additional signal output from K-RasG12V S181A nanoclusters is unable to further potentiate PC12 differentiation. Intriguingly, K-RasG12V S181D generates the highest level of ppERK, which is associated with a significant increase in the proportion of PC12 cells undergoing differentiation. On one level, this observation is seemingly at odds with the reduced K-RasG12V S181D plasma membrane nanocluster formation. However, the K-RasG12V S181D nanoclusters are functional, as shown by Raf-1 plasma membrane recruitment and nanoclustering. The increased signal output from K-RasG12V S181D may reflect combined output from plasma membrane nanoclusters and additional Raf/MEK/ERK signaling platforms on internal membranes such as the mitochondria (1). If these signals are additive, then the combined total cellular signal output generated by K-RasG12V S181D will be greater than those of K-RasG12V and K-RasG12V S181A. Thus, it is conceivable that K-RasG12V S181D achieves maximal signal output from plasma membrane nanoclusters and additional signal strength is generated from signaling platforms on intracellular membranes. Thus, we propose that the response of PC12 cells is the net result of the combined total cellular signal output, which is determined by the range of the signaling platforms accessible to K-Ras. Alternatively, changes to the composition or dynamics of the K-RasG12V S181D plasma membrane nanocluster may account for the modified signal output. In this scenario, K-RasG12V S181D generates a unique signal output that is capable of promoting extensive differentiation. Taken together, these data suggest that K-Ras–GTP nanocluster formation and function are regulated by a complex interplay between the charge of the polybasic domain and the lipid environment.

We have shown previously that there is a linear relationship between the number of K-Ras–GTP nanoclusters on the plasma membrane and the stimulating EGF concentration (25). This relationship is critical for high-fidelity analog signaling across the plasma membrane, with the slope of the actual system EGF-ppERK dose response being determined by the K-Ras clustered fraction (25). Therefore, the finding that the number of K-Ras–GTP nanoclusters can be physiologically modulated by PKC-mediated phosphorylation of Ser181 suggests that PKC may have a novel role in regulating signal gain through the MAPK pathway.

In summary, we have shown that Ras nanocluster composition regulates effector recruitment and highlighted the importance of lipid/protein nanoscale environments to the activation of signaling cascades. Different Ras nanoclusters therefore generate quantitatively different signal outputs. Furthermore, physiological regulation of nanocluster formation offers additional levels of control over the magnitude of signal output from complexes that use nanoclusters as signaling platforms.

ACKNOWLEDGMENTS

This work was supported by grants to J.F.H. from the National Institutes of Health (GM-066717), the National Health and Medical Research Council, and the Queensland Cancer Fund. The IMB is a Special Research Centre of the Australian Research Council.

Downloaded from http://mcb.asm.org/ on October 26, 2015 by University of Queensland Library

REFERENCES

1. **Bivona, T. G., S. E. Quatela, B. O. Bodemann, I. M. Ahearn, M. J. Soskis, A. Mor, J. Miura, H. H. Wiener, L. Wright, S. G. Saba, D. Yim, A. Fein, I. Perez de Castro, C. Li, C. B. Thompson, A. D. Cox, and M. R. Philips.** 2006. PKC regulates a farnesyl-electrostatic switch on K-Ras that promotes its association with Bcl-Xl on mitochondria and induces apoptosis. Mol. Cell **21:**481–493.
2. **Cales, C., J. F. Hancock, C. J. Marshall, and A. Hall.** 1988. The cytoplasmic protein GAP is implicated as the target for regulation by the ras gene product. Nature **332:**548–551.
3. **Clayton, A. H., Q. S. Hanley, and P. J. Verveer.** 2004. Graphical representation and multicomponent analysis of single-frequency fluorescence lifetime imaging microscopy data. J. Microsc. **213:**1–5.
4. **Diggle, P. J., J. Mateu, and H. E. Clough.** 2000. A comparison between parametric and non-parametric approaches to the analysis of replicated spatial point patterns. Adv. Appl. Prob. (SGSA) **32:**331–343.
5. **Esposito, A., H. C. Gerritsen, and F. S. Wouters.** 2005. Fluorescence lifetime heterogeneity resolution in the frequency domain by lifetime moments analysis. Biophys. J. **89:**4286–4299.
6. **Ghosh, S., J. C. Strum, V. A. Sciorra, L. Daniel, and R. M. Bell.** 1996. Raf-1 kinase possesses distinct binding domains for phosphatidylserine and phosphatidic acid. Phosphatidic acid regulates the translocation of Raf-1 in 12-O-tetradecanoylphorbol-13-acetate-stimulated Madin-Darby canine kidney cells. J. Biol. Chem. **271:**8472–8480.
7. **Ghosh, S., W. Q. Xie, A. F. Quest, G. M. Mabrouk, J. C. Strum, and R. M. Bell.** 1994. The cysteine-rich region of raf-1 kinase contains zinc, translocates to liposomes, and is adjacent to a segment that binds GTP-ras. J. Biol. Chem. **269:**10000–10007.
8. **Gorfe, A. A., M. Hanzal-Bayer, D. Abankwa, J. F. Hancock, and J. A. McCammon.** 2007. Structure and dynamics of the full-length lipid-modified H-Ras protein in a 1,2-dimyristoylglycero-3-phosphocholine bilayer. J. Med. Chem. **50:**674–684.
9. **Hancock, J. F., and R. G. Parton.** 2005. Ras plasma membrane signaling platforms. Biochem. J. **389:**1–11.
10. **Hancock, J. F., H. Paterson, and C. J. Marshall.** 1990. A polybasic domain or palmitoylation is required in addition to the CAAX motif to localize p21ras to the plasma membrane. Cell **63:**133–139.
11. **Hekman, M., H. Hamm, A. V. Villar, B. Bader, J. Kuhlmann, J. Nickel, and U. R. Rapp.** 2002. Associations of B- and C-Raf with cholesterol, phosphatidylserine, and lipid second messengers: preferential binding of Raf to artificial lipid rafts. J. Biol. Chem. **277:**24090–24102.
12. **Herrmann, C., G. A. Martin, and A. Wittinghofer.** 1995. Quantitative analysis of the complex between p21ras and the Ras-binding domain of the human Raf-1 protein kinase. J. Biol. Chem. **270:**2901–2905.
13. **Hibino, K., T. M. Watanabe, J. Kozuka, A. H. Iwane, T. Okada, T. Kataoka, T. Yanagida, and Y. Sako.** 2003. Single- and multiple-molecule dynamics of the signaling from H-Ras to cRaf-1 visualized on the plasma membrane of living cells. Chemphyschem **4:**748–753.
14. **Leevers, S. J., H. F. Paterson, and C. J. Marshall.** 1994. Requirement for Ras in Raf activation is overcome by targeting Raf to the plasma membrane. Nature **369:**411–414.
15. **Leventis, R., and J. R. Silvius.** 1998. Lipid-binding characteristics of the polybasic carboxy-terminal sequence of K-ras4B. Biochemistry **37:**7640–7648.
16. **McPherson, R. A., A. Harding, S. Roy, A. Lane, and J. F. Hancock.** 1999. Interactions of c-Raf-1 with phosphatidylserine and 14-3-3. Oncogene **18:**3862–3869.
17. **Murakoshi, H., R. Iino, T. Kobayashi, T. Fujiwara, C. Ohshima, A. Yoshimura, and A. Kusumi.** 2004. Single-molecule imaging analysis of Ras activation in living cells. Proc. Natl. Acad. Sci. USA **101:**7317–7322.
18. **Plowman, S. J., C. Muncke, R. Parton, and J. F. Hancock.** 2005. H-ras, K-ras and inner plasma membrane raft proteins operate in nanoclusters with differential dependence on the actin cytoskeleton. Proc. Natl. Acad. Sci. USA **102:**15500–15505.
19. **Prior, I. A., C. Muncke, R. G. Parton, and J. F. Hancock.** 2003. Direct visualization of Ras proteins in spatially distinct cell surface microdomains. J. Cell Biol. **160:**165–170.
20. **Rotblat, B., I. A. Prior, C. Muncke, R. G. Parton, Y. Kloog, Y. I. Henis, and J. F. Hancock.** 2004. Three separable domains regulate GTP-dependent association of H-ras with the plasma membrane. Mol. Cell. Biol. **24:**6799–6810.
21. **Roy, S., R. Luetterforst, A. Harding, A. Apolloni, M. Etheridge, E. Stang, B. Rolls, J. F. Hancock, and R. G. Parton.** 1999. Dominant-negative caveolin inhibits H-Ras function by disrupting cholesterol-rich plasma membrane domains. Nat. Cell Biol. **1:**98–105.
22. **Roy, S., S. J. Plowman, B. Rotblat, I. A. Prior, C. Muncke, S. Grainger, R. G. Parton, Y. I. Henis, Y. Kloog, and J. F. Hancock.** 2005. Individual palmitoyl residues serve distinct roles in H-Ras trafficking, microlocalization, and signaling. Mol. Cell. Biol. **25:**6722–6733.
23. **Silvius, J. R., P. Bhagatji, R. Leventis, and D. Terrone.** 2006. K-ras4B and prenylated proteins lacking "second signals" associate dynamically with cellular membranes. Mol. Biol. Cell **17:**192–202.
24. **Stokoe, D., S. G. Macdonald, K. Cadwallader, M. Symons, and J. F. Hancock.** 1994. Activation of Raf as a result of recruitment to the plasma membrane. Science **264:**1463–1467.
25. **Tian, T., A. Harding, K. Inder, S. Plowman, R. G. Parton, and J. F. Hancock.** 2007. Plasma membrane nanoswitches generate high-fidelity Ras signal transduction. Nat. Cell Biol. **9:**905–914.
26. **Verveer, P. J., and P. I. Bastiaens.** 2003. Evaluation of global analysis algorithms for single frequency fluorescence lifetime imaging microscopy data. J. Microsc. **209:**1–7.
27. **Wang, J., A. Gambhir, G. Hangyas-Mihalyne, D. Murray, U. Golebiewska, and S. McLaughlin.** 2002. Lateral sequestration of phosphatidylinositol 4,5-bisphosphate by the basic effector domain of myristoylated alanine-rich C kinase substrate is due to nonspecific electrostatic interactions. J. Biol. Chem. **277:**34401–34412.
28. **Wellbrock, C., M. Karasarides, and R. Marais.** 2004. The RAF proteins take centre stage. Nat. Rev. Mol. Cell Biol. **5:**875–885.
29. **Yan, J., S. Roy, A. Apolloni, A. Lane, and J. F. Hancock.** 1998. Ras isoforms vary in their ability to activate Raf-1 and phosphoinositide 3-kinase. J. Biol. Chem. **273:**24052–24056.

Downloaded from http://mcb.asm.org/ on October 26, 2015 by University of Queensland Library